Development and evaluation of molecular imaging probes for CXCR4 mediated chemotaxis and tumor infiltration of activated T-Cells

Hartimath, Siddanna Vrushabendra Swamy

Chapter 2:

$[^{99m}Tc]O_2$-AMD3100 as a SPECT Tracer for CXCR4 Receptor Imaging

S V. Hartimath[1], Urszula M. Domanska[2], Annemiek M.E. Walenkamp[2], R.A.J.O. Dierckx[1], Erik F.J. de Vries[1]

[1]Departments of Nuclear Medicine and Molecular imaging,

[2]Medical Oncology, University Medical centre Groningen, University of Groingen, Groningen, The Netherlands

NUCL MED BIOL: 2013; 40(4):501-15

ABSTRACT

CXCR4 plays an important role in HIV infection, tumor progression, neurogenesis, and inflammation. *In-vivo* imaging of CXCR4 could provide more insight in the role of this receptor in health and disease. The aim of this study was to investigate [^{99m}Tc]O_2-AMD3100 as a potential SPECT tracer for imaging of CXCR4. AMD3100 was labelled with sodium [^{99m}Tc]pertechnetate. A cysteine challenge assay was performed to test the tracer stability. Heterologous and homologous receptor binding assay and internalization assay were performed in CXCR4 expressing Jurkat-T cells. *Ex vivo* biodistribution was studied in healthy mice at 30, 60, and 120 min after tracer injection. Tumor uptake of the tracer was determined by microSPECT imaging in nude mice xenografted with human PC-3 prostate tumor. Specific uptake of tracer was determined by blocking studies using an excess of unlabelled AMD3100. AMD3100 was labelled with technetium-99m with a radiochemical yield of >98%. The tracer was stable in PBS and mouse plasma for at least 6 h at 37^{0}C. Heterologous and homologous binding assays with AMD3100 showed IC_{50} values of 240 ± 10 μM, and 92 ± 5 μM for [^{125}I]SDF-1α and [^{99m}Tc]O_2-AMD3100 respectively, with negligible receptor internalisation. The tracer showed high uptake in liver, lungs, spleen, thymus, intestine and bone. Blocking dose of AMD3100.8HCl (20mg/kg) decreased the uptake in these organs (p<0.05). [^{99m}Tc]O_2 -AMD3100 showed specific tumor accumulation in mice bearing PC-3 xenografts model. Time activity curves (TAC) in AMD3100 pre-treated animals tracer showed 1.7 times less tumor uptake as compared to control animals (p<0.05). [^{99m}Tc]O_2-AMD3100 is readily labelled, is stable in plasma and displays a favourable binding affinity for the CXCR4 receptors. [^{99m}Tc]O_2-AMD3100 shows specific binding in organs with high CXCR4 expression and in CXCR4 positive tumors. These results justify further evaluation of this radiopharmaceutical as a potential biomarker for the non-invasive imaging of CXCR4 receptors.

INTRODUCTION

The chemokine receptor 4 (CXCR4) is a member of the α-chemokine family and belongs to a larger superfamily of receptors known as G protein coupled receptors (GPCRs). Stromal cell-derived factor 1α (SDF-1α/CXCL12) is the natural ligand for CXCR4 receptors. CXCR4 is widely expressed by hematopoietic and non-hematopoietic cell types, including T cells, B cells, neutrophils, monocytes, CD34+ cells, endothelial cells, neurons, and astrocytes. CXCR4 and CXCL12 play an important role in the regulation of leukocyte trafficking, hematopoiesis, angiogenesis, cancer, and viral pathogenesis [1-7]. In addition, CXCR4 and its cognate ligand are also expressed in the brain, where they are involved in development, migration, differentiation, neuroplasticity and proliferation of glia and neuronal cells. Recently, possibility has been raised that CXCR4 and CXCL12 might act as neurotransmitter or neuromodulator [8-10]. Both CXCR4 and CXCL12 knockout mice show loss of functioning B cells, vascularisation, and abnormal development of brain areas such as hippocampus, neocortex, and cerebellum [3, 11, 12].

CXCL12 and its receptor CXCR4 mediate the recruitment of immune cells to sites of inflammation and infection. Consequently, they are upregulated in several disease conditions, including allergy, infectious diseases, atherosclerosis, multiple sclerosis, rheumatoid arthritis, and psoriasis [13-15]. CXCR4 and CCR5 were discovered to serve as the principal co-receptors that mediate the entry of the human immunodeficiency virus (HIV) into the immune cells [16]. It has been proposed that HIV-induced neuronal death and dementia could be mediated by CXCR4 as HIV co-receptors [17-19]. The expression of CXCR4 receptors in various physiological and pathological conditions makes them potential candidates for drug development.

Apart from their role in immune response and infection, CXCR4 receptors also play a significant role in tumor growth and metastasis. More than 20 different kinds of human tumors overexpress CXCR4 and CXCL12 [6, 20-22]. An increased expression of CXCR4 and its ligand CXCL12 is associated with a high risk of metastases [23-25]. This could make CXCR4 an important biomarker to identify primary tumors that are

likely to metastasize [26, 27]. Furthermore, the overexpression of these chemokine receptors can play a role in the metastatic destination of tumor cells [28, 29]. Inhibition of CXCR4/CXCL12 signalling resulted in reduced metastatic potential in various animal tumor models [30-32]. As a consequence, a number of CXCR4 inhibitors are now under clinical investigation.

Non-invasive imaging modalities can provide a better understanding of the role of CXCR4 in health and disease. For example, an *in vivo* imaging tool might be helpful to identify patients with tumors expressing high levels of the CXCR4 receptor, thus likely to respond to CXCR4 based therapies. Such a tool can also be utilised for early diagnosis and treatment response monitoring of CXCR4 positive tumors. A number of attempts have been made to non-invasively image CXCR4 receptors, using nuclear imaging techniques. As a result, several positron emitting tomography (PET) and single photon emitting computed tomography (SPECT) based imaging probes for CXCR4 expression have been evaluated in animal cancer models [33-37]. AMD3100 is a specific and selective CXCR4 receptor antagonist; it is a prototype non-peptide, small molecule inhibitor [38]. AMD3100 has been used in clinical trials as an anti-HIV therapy [39]. In addition, it was shown to be an effective mobiliser of hematopoietic stem cells in healthy volunteers and in multiple myeloma and non-Hodgkin's lymphoma patients [40, 41]. Furthermore, AMD3100 effectively inhibits autoimmune collagen-induced arthritis, neuroinflammation and asthma in animal models [42]. Compelling evidence suggests that the aspartic acid residues Asp171 and Asp262 of CXCR4 play a key role in the interaction between receptors and AMD3100 [43]. Recently, a brief communication on imaging of CXCR4 by SPECT agent [^{99m}Tc]O_2-AMD3100 was published, but proper *in-vitro* and *in-vivo* evaluation has not been described so far [44]. In this paper, we report the radiolabeling and quality control of [^{99m}Tc]O_2-AMD3100. Furthermore, we describe here the *in-vitro* and *in-vivo* evaluation of [^{99m}Tc]O_2-AMD3100 as a SPECT tracer for CXCR4.

MATERIALS AND METHODS

All the reagents and solvents were purchased from Sigma Aldrich chemical company and used without further purification. ^{1}H NMR was acquired with a Varian Oxford 400 MHz NMR instrument. Recombinant CXCL12 was purchased from R&D System. Na[^{99m}Tc]O_4 was produced by elution of the ^{99}Mo/^{99m}Tc generator according to the manufacturer's instructions. Carrier-free sodium iodide [Na^{125}I] in phosphate buffer was obtained from MDS Nordion. AMD3100 octahydrochloride hydrate (AMD3100.8HCl) was prepared according to a method previously described in the literature [35, 38, 45, 46].

Labelling of AMD3100 with Na^{99m}TcO$_4$

Radiolabeling of AMD3100 was performed with sodium [^{99m}Tc] pertechnetate in the presence of stannous chloride ($SnCl_2$). In brief, 10 µL of the AMD3100 solution (10 mg/mL in H_2O) and 300 µl of $SnCl_2.2H_2O$ solution (1 mg/mL in water) were prepared freshly and added to the reaction vial. The pH of the solution was adjusted to 7.2 with 1 M sodium citrate buffer (~ 5 µL). Sodium[^{99m}Tc] pertechnetate (400 MBq) was added to the mixture and incubated for 20 min at room temperature [44]. For the determination of conversion and radiochemical purity, samples were analysed by radio-thin layer chromatography (RTLC) using Whatman paper No. 3. RTLC analyses were performed using 0.9 % NaCl, methyl ethyl ketone (MEK) or ammonia: water: ethanol (1:5:5) as the mobile phase. To obtain the optimum labelling yield of the [^{99m}Tc]O_2-AMD3100 complex, the reaction conditions were optimised for different parameters, such as the concentrations of AMD3100 and $SnCl_2$, incubation period and the pH of the reaction mixture. The tracer was diluted with PBS (pH 7.4) to obtain the required concentration for cell and animal experiments (Fig-1).

Labelling of [^{125}I] SDF-1α

[^{125}I]SDF-1α was prepared by reaction of SDF-1α with sodium [^{125}I] iodide in the presence of N-bromosuccinimide (NBS) as a mild oxidizing agent [47]. Prior to iodination, the SDF-1α was dissolved in PBS at a final concentration of 1 mg/mL. The NBS solution in water (0.25 mg/mL) was prepared freshly. The reaction mixture

was prepared by mixing 50 µL of SDF-1α (5 µg), 25 µL tris buffer (pH 7.4), 20 µL (40 MBq) sodium [^{125}I]iodide and 10 µL of freshly prepared NBS. The mixture was vortexed for 30 s and allowed to stand for 5 min at room temperature. After the reaction was stopped by dilution with PBS, the labelled protein was separated from free [^{125}I]iodide using a PD-10 size exclusion cartridge (GE, Healthcare) that was pre-conditioned with PBS. The column was eluted with PBS and the fraction with maximum amount of radioactivity was collected and stored for further use. The percentage of free [^{125}I] iodide was determined using a trichloroacetic acid (TCA) precipitation assay. The percentage of free [^{125}I] iodide was found to be less than 1%.

Partition co-efficient

To a mixture of 0.5 mL *n*-octanol and 0.5 mL of sterile water, 10 µL of the tracer solution was added, and the biphasic solution was mixed well. The mixture was incubated at 37^{0}C for 1 h and subsequently centrifuged at 3000 rpm for 5 min. 100 µL aliquots were collected from each layer and radioactivity was counted in a γ-counter (Compugamma CS1282, LKB-Wallac, Turku, Finland). The log value of the octanol–water partition coefficient is reported as the average of three independent experiments.

In-vitro stability

The stability of the [^{99m}Tc]O_2-AMD3100 complex was measured by diluting a solution containing more than 98% pure [^{99m}Tc]O_2-AMD3100 complex with PBS or mouse plasma. For this purpose, fresh blood samples were collected from mice. After the blood was centrifuged at 3000 rpm, plasma was collected and divided into 250 µL aliquots. 10 µL of [^{99m}Tc]O_2-AMD3100 was added to 240 µL of fresh plasma or PBS and incubated at 37^{0}C. The percentages of free and AMD3100 bound ^{99m}Tc were measured at different time points (1, 2, 4, 6, and 24 h) by RTLC. In addition, a cysteine challenge assay was performed in order to check the *in vitro* stability of the complex. The tracer was incubated at 37^{0}C for 60 min at different cysteine to AMD3100 molar ratios (up to 500:1). At the end of the incubation time, the reaction mixture was analysed by RTLC as described above. Furthermore, stability

of tracer in 0.5 M NaOH and HCl was evaluated by incubating tracer up to 3 h at room temperature.

Cell cultures

The CXCR4-positive Jurkat-T and PC-3 cell lines were purchased from ATCC (Manassas, VA, USA). Jurkat-T and PC-3 cells were cultured in RPMI-1640 supplemented with 10% FCS. Cells were maintained at 37^0C in humidified 5% CO_2 atmosphere.

In vitro receptor binding assays

Both heterologous and homologous competition binding assays were performed on Jurkat-T cells in order to test the specific binding [34-36, 48]. Cells were harvested and seeded in 12-well plates at a density of 10^6 cells per well. After 24 h, the cells were washed twice with PBS. The heterologous binding assay was performed by adding an increasing concentration of unlabelled AMD3100 in the range of $10^{-6} - 10^{-3}$ M to the cells, followed by incubation with 100 pM [^{125}I]-SDF-1α in a 1000 µL binding buffer (PBS pH 7.4, supplemented with 50 mM HEPES, 5 mM $MgCl_2$, 1 mM $CaCl_2$, 0.5% BSA) for 3 h at 4^0C. After incubation, cells were quickly washed two times with 500 µL cold binding buffer and cell-associated radioactivity was measured by an automated gamma counter. Similarly, a homologous binding assay was done using 100 nM of [^{99m}Tc]O_2-AMD3100. Cells were incubated for 1 h at 37^0C in 1000 µL binding buffer (PBS containing, 5 mM $MgCl_2$, 1 mM $CaCl_2$, 0.5% BSA). The IC_{50} values were determined by nonlinear regression analysis, using GraphPad Prism 5.0. All experiments were performed in triplicate.

Receptor internalization assay

Jurkat-T cells were seeded in 6-well plates (10^6 cells per well). After 24 h cells were washed two times with PBS. Cells were incubated with [^{99m}Tc]O_2-AMD3100 for 2 h at 4^0C. Unbound radioactivity was removed by washing with cold PBS. Cells were then incubated with pre-warmed binding buffer and incubated at 37^0C for different time intervals to allow for receptor internalization. The membrane bound tracer was removed by washing with acid buffer (50 mM glycine-HCl, 10 mM NaCl, pH 2.8). The cells were washed twice with ice-cold binding buffer and subsequently

lysed with 1 M NaOH at 37^0C. The lysate was collected to determine the internalization fraction. The radioactivity in each fraction was measured with a γ-counter and the percentage internalization was calculated according to the formula:

% Internalization = [activity in lysate/(activity in lysate + activity in membrane bound fraction)] * 100%.

Animals

Male Balb/*c* mice (3–4 weeks old) were obtained from Harlan (Lelystad, The Netherlands). The animals were provided with standard laboratory food and water. All the animal studies were approved by the institutional ethics committee for Animal Research, of the University of Groningen (DEC protocol No. 6073A) and executed in accordance with the regulations of Dutch law on animal welfare. The immune-competent wild type Balb/*c* mice were used for *ex vivo* biodistribution to provide information about tracer uptake in immune-related organs, whereas tumors bearing male Balb/*c* Athymic *nu/nu* immune-compromised animals were used for *in vivo* SPECT imaging to demonstrate tumor targeting of the tracer. Human PC-3 prostate tumor cells were grafted in nude athymic Balb/*c* mice by subcutaneous inoculation, PC-3 cells (2×10^6 cells) in a 1:1 mixture of matrigel and RPMI-1640 medium containing 10% FCS were injected subcutaneously into the right front flank. Xenografts were allowed to grow during a period of 2–3 weeks; the tumor size was measured weekly using vernier calliper. When the tumor volume had reached a size of about 200 ± 25 mm^3 (weight of the tumor at end of scan 250 ± 10 mg n = 6), the animals were used for SPECT imaging.

Biodistribution studies

Sixteen healthy Balb/*c* mice were randomly divided into four groups of four animals. Isoflurane (1.5% in medical air) inhalation was used as method of anesthesia during injection of the tracer. All groups were injected with 5-10 MBq of [^{99m}Tc]O_2-AMD3100 via the penile vein. At 30, 60, or 120 min post injection (group 1, 2 and 3 respectively), the animals were sacrificed and various organs of interest (heart, liver, spleen, lung, blood cells, bone, thymus, pancreas, small and large

intestine, stomach, kidney and bladder) were harvested and weighed. The radioactivity in these tissues was determined with a γ-counter.

In order to determine the specific binding of the tracer, four mice (group 4) were injected with a blocking dose of AMD3100.8HCl (20 mg/kg, s.c) 30 min before injection of the radiotracer. One hour after injection of the tracer, the animals were sacrificed. Blood and organs were collected, weighed, and counted as described above. Tracer uptake is expressed as a percentage of injected dose/gram of tissue (% ID/g).

MicroSPECT Imaging

Imaging experiments were performed on PC-3 xenograft bearing Athymic *nu/nu* mice (n = 6). After the animals were anaesthetized with 1.5% of isoflurane in medical air, [^{99m}Tc]O_2-AMD3100 (60 ± 10 MBq) was injected intravenously via the penile vein. Immediately after tracer injection, the animals were placed in a prone position in a three-headed SPECT camera (MILabs, U-SPECT-II, Utrecht, The Netherlands) equipped with a multi-pinhole high-resolution collimator (pinhole diameter 0.6 mm, spatial resolution about 0.4 mm). The field of view was set to include the tumor and its immediate surroundings. Immediately after positioning of the animal, dynamic data were acquired for 60 min (12 frames, 5 min per frame). Subsequently, a whole body static image was collected over a period of 10 min. The imaging data were stored digitally in list mode.

The SPECT imaging study was performed as a longitudinal experiment, in which each animal was scanned twice. On day 1, animals were investigated under baseline conditions. On day 2, the SPECT scan was repeated on the same animal after a blocking dose of unlabeled AMD3100.8HCl (20 mg/kg) was administered s.c 30 min before tracer injection. The imaging data were acquired using the same procedure as described above. Only after the second scan, animals were terminated and tumor and other organs were collected for histopathological analysis.

Images were reconstructed with U-SPECT-Rec v 1.34i3 software (MILabs, Utrecht, The Netherlands) with a pixel-based ordered subsets expectation maximum (POSEM) algorithm. The SPECT images of the tumor bearing mice were loaded in

the Inveon analysis software (Siemens). Regions of interest were drawn around the tumor on all slices that showed part of the tumor. Thus, a volume of interest was generated by combining the 2 dimensional ROIs. The radioactivity concentration in the volume of interest was measured and converted to % ID/g by correction for the injected dose. It is assumed that 1 mm^3 of tissues equals 1 g. Results are expressed as mean ± SD.

Immunohistochemistry

Tumor and other organs from the imaging experiments were collected, snap-frozen in liquid nitrogen and stored in a freezer at −80^{0}C until required for further use. All the tissues were cut in 5-µm thick sections for HE and immunostaining. The sections were fixed in acetone and immersed in PBS solution containing 0.5% hydrogen peroxidase for 30 min to block endogenous peroxidase activity. The sections were then incubated in 2.5% normal serum to reduce non-specific binding, and then sections were incubated overnight at 4^{0}C with primary rabbit polyclonal anti-CXCR4 antibody (Abcam, clone 2074; Cambridge, UK) at a dilution of 1:500. A negative control without the primary antibody was included to check the specificity of the antibody. The sections were processed using standard horseradish peroxidase (HRP) conjugated secondary and tertiary antibody according to the manufacturer's recommendations (Dako, Belgium). Diaminobenzidine (DAB) was used as a chromogen, and hematoxylin was used for counterstaining. After washing, cover slips were mounted and sections were examined under a Leica microscope.

Statistical analysis

Statistical analyses were performed using Excel 2010 (Microsoft) and GraphPad prism 5. All the data represent the mean ± SD, differences in tracer accumulation between controls and the AMD3100 treated group were analyzed using an unpaired two-sided student's *t-test* in case of biodistribution and a paired two-sided student's *t-test* for the imaging studies. Data were considered statistically significant when *p* values were smaller than 0.05.

RESULTS

Radiolabelling of AMD3100

Although radiolabelling of macrocyclic cyclams with [^{99m}Tc] pertechnetate has been reported in the literature [Fig-1, 44, 49, 50]. We first aimed to optimize the labelling parameters for the incorporation of ^{99m}Tc into the bicyclam under reducing conditions. To achieve an optimum yield of [^{99m}Tc]O_2-AMD3100, effects of pH, concentration of $SnCl_2$ and AMD3100 were investigated. Labelling yield was strongly dependent on pH, as labelling efficiencies of 19% ± 3% (n = 5), 97% ± 2% (n = 5) and 26% ± 1% (n = 5) were obtained when a 1 M citrate buffer at pH 3, 7 and 11 was used, respectively. The effect of stannous chloride concentration on radiolabeling was studied in the range of 10^{-5} M to10^{-1} M. Fig-2A shows that the radiolabeling yield increases with an increasing stannous chloride concentration, reaching a plateau at 10^{-3} M with a maximum yield of > 98%. Similarly, the effect of AMD3100 concentration was determined using amounts of the ligand that ranged from 10^{-6} M to 10^{-2} M. An increasing yield was observed as a function of increasing concentrations of AMD3100 until a plateau was reached at 10^{-4} M, corresponding to a maximum labelling yield of >98% (Fig-2B). Under optimal reaction conditions (pH 7, 0.5 mM $SnCl_2$, 0.135 mM AMD3100, reaction time 20 min at room temperature), a labelling yield of 98 ± 1% was achieved, with a specific activity of 8600±200 MBq/µM. These conditions were used for labelling of AMD3100 for the *in-vitro* and *in- vivo* experiments.

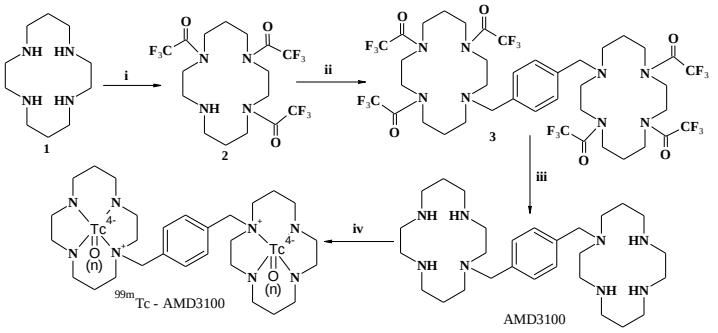

Figure-1: Synthesis of AMD3100 and radiolabelling: Reagents and conditions (i) ethyl trifloroacetate, triethylamine, MeOH, room temperature, overnight (ii) α,α-dibromoxylene, K_2CO_3, CH_3CN, reflux, over-night. (iii) K_2CO_3, methanol reflux 6hr. (iv) $SnCl_2$, $Na^{99m}TcO_4$, pH7, 20 min RT.

Quality control and characterization of [^{99m}Tc]O_2-AMD3100

The quality control of [^{99m}Tc]O_2-AMD3100 was performed by TLC using Whatman No. 3 paper. When 0.9% NaCl was used as the solvent, retention factors (R_f) were 0.81 ± 0.02 for [^{99m}Tc]O_2-AMD3100 and 0.86 ± 0.01 for free Na[^{99m}Tc]O_4. When 2-butanone was used as the solvent, R_f were as follows: 0.11 ± 0.06 [^{99m}Tc]O_2AMD3100 and, 0.89 ± 0.06 for free Na[^{99m}Tc]O_4. In order to determine the presence of reduced hydrolysed technetium colloids (TcO^{-2}), TLC was performed in ammonia: water: ethanol (1:5:5). The colloids remained at the origin, while the AMD3100 complex along with free [^{99m}Tc] pertechnetate migrated with the solvent

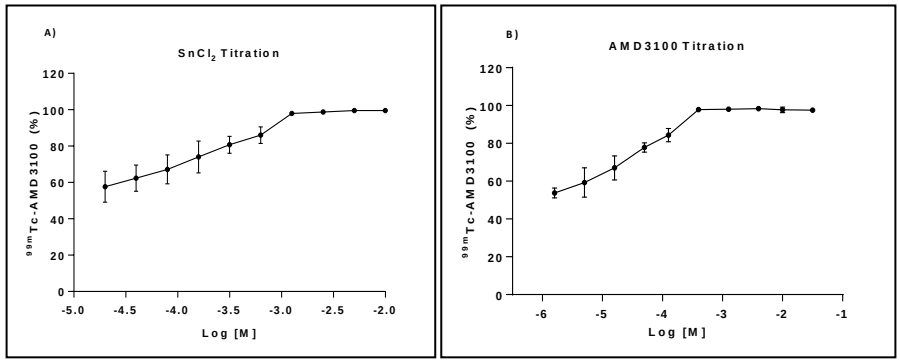

Figure- 2: A) Labelling yield as function of $SnCl_2$ concentration. Conditions: concentration AMD3100 0.135×10^{-3} M, pH 7, incubation time 20 min, temperature 25^0C. B) Labelling yield as function of AMD3100 concentration. Conditions: concentration $SnCl_2$ 0.5×10^{-3} M, pH 7, incubation time 20 min, temperature 25^0C.

front. After the optimisation of reaction, the formation of the colloids (TcO^{-2}) and free [^{99m}Tc] pertechnetate was found to be less than 1% in total, whereas the amount of [^{99m}Tc]O_2-AMD3100 was >99%. Hence, we decided that further purification of the tracer by HPLC was not required. The partition coefficient of the tracer was determined in a mixture of *n*-octanol and water. The *logP* value was found to be −2.60 ± 0.25, this indicates that the tracer is highly hydrophilic.

The *in vitro* stability of the [^{99m}Tc]O_2-AMD3100 complex was studied in PBS and mouse plasma at different time intervals. The tracer was stable in PBS and plasma for at least 6 h at 37^0C (Fig-3A). After 24 h, still 60% tracer was intact in PBS, whereas about 35% was still intact in mouse plasma. In addition, the stability of the preparation was tested in a challenge assay, in which the tracer was incubated with

an increasing amount of cysteine at 37^{0}C for 1 h. Negligible decomposition of [^{99m}Tc]O_2-AMD3100 was observed when the complex was incubated with up to 50-fold excess of cysteine. Even when the labelled complex was exposed to a 500-fold excess of cysteine, it only released 20% of the activity (Fig-3B). Furthermore, >90% of the tracer was still intact, when it was incubated with 0.5 M NaOH or 0.5 M HCl for 1 h at room temperature. However, there was a significant loss of the integrity of the tracer after 3 h of incubation (data not shown). Taken together, [^{99m}Tc]O_2-AMD3100 was considered sufficiently stable for further evaluation.

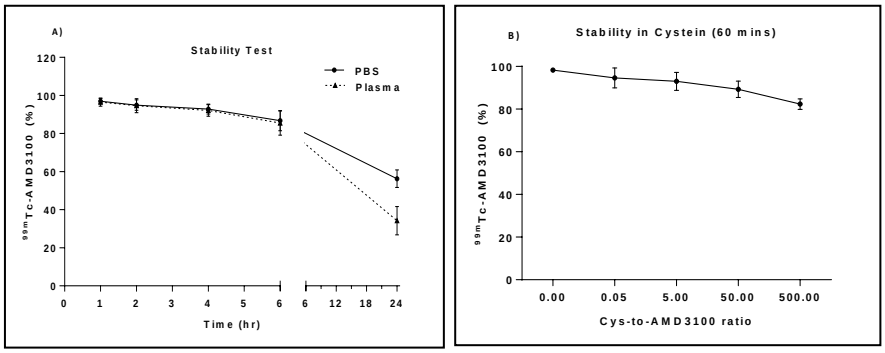

Figure-3: A) *In vitro* stability test of [^{99m}Tc]O_2-AMD3100 in PBS and mouse plasma at 37^{0}C for different time points. B) Cysteine challenge assay of [^{99m}Tc]O_2-AMD3100 at increasing molar ratio of cysteine to AMD3100 incubation 60 min at 37^{0}C.

In-vitro binding and internalization

The Jurkat-T cell line naturally expresses CXCR4 [35]. To study the binding of the radiopharmaceutical to CXCR4 receptor, a heterologous and a homologous binding assay was performed in Jurkat-T cells, using [^{125}I]SDF-1α and [^{99m}Tc]O_2-AMD3100 as the CXCR4 specific radioligand, respectively. Radioligand binding was plotted in sigmoid curves for the both radioligands as a function of increasing concentration of AMD3100 (Fig-4A). The measured IC_{50} values were 240 ± 10 µM, and 92 ± 5 µM for [^{125}I]SDF-1α and [^{99m}Tc]O_2-AMD3100, respectively. The binding and internalization assays showed that tracer binding to the cell membrane bound receptor reaches a plateau in 60 min (Fig-4B). In addition, there is hardly any cytosolic accumulation of tracer after an incubation period of 4 h, indicating that internalization of the receptors after binding of the tracer is negligible.

Ex vivo biodistribution

The results of the *ex vivo* biodistribution of [^{99m}Tc]O_2-AMD3100 in healthy mice is shown in Fig-5A. The percentage of injected dose/gram of tissues (% ID/g) of the tracer was determined in various organs at 30, 60, and 120 min post injection. In immune-related organs with a high density of CXCR4 expressing cells, such as the bone (marrow), spleen, liver and thymus, tracer uptake was highest at 1 h post injection and decreased thereafter, with most activity being eliminated by 2 h. Hepatic uptake was modest, wherease accumulation in the kidney and bladder (6%

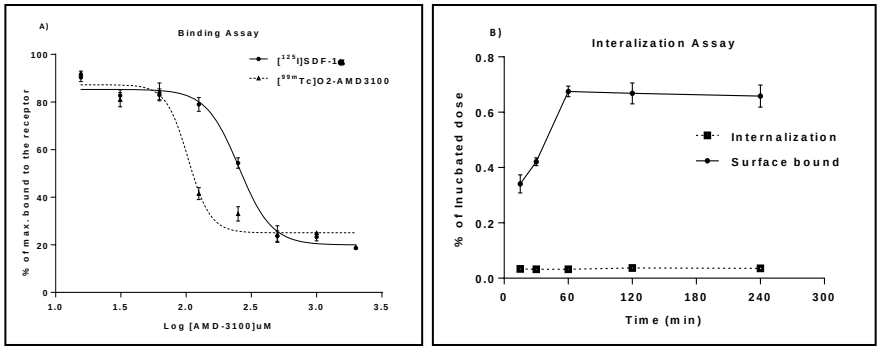

Figure- 4: A) *In vitro* heterologous and homologous AMD3100 displacement assay with [^{125}I]SDF-1α and [^{99m}Tc]O_2-AMD3100, respectively. The experiment was performed in triplicate. B) Receptor internalization assay in Jurkat-T cells. Cells were incubated with [^{99m}Tc]O_2-AMD3100 for 1 h at 4^{0}C. Cells were subsequently washed and warmed at 37^{0}C for the indicated time points to permit the internalization of receptors.

and 58% ID/g respectively) was high, due to rapid clearance of radioactivity from the blood pool via renal–urinary route. Moreover, negligible accumulation was detected in brain and muscle. When the uptake over time was evaluated, only the kidney and bladder showed increased tracer uptake for at least 2 h. The administration of a blocking dose of AMD3100 resulted in a decrease in uptake of the tracer (Fig-5B) in organs such as liver (61%), intestine (72%), thymus (91%), spleen (62%), and bone (52%). This reduction of tracer uptake was statically significant ($p < 0.05$) in all of these organs.

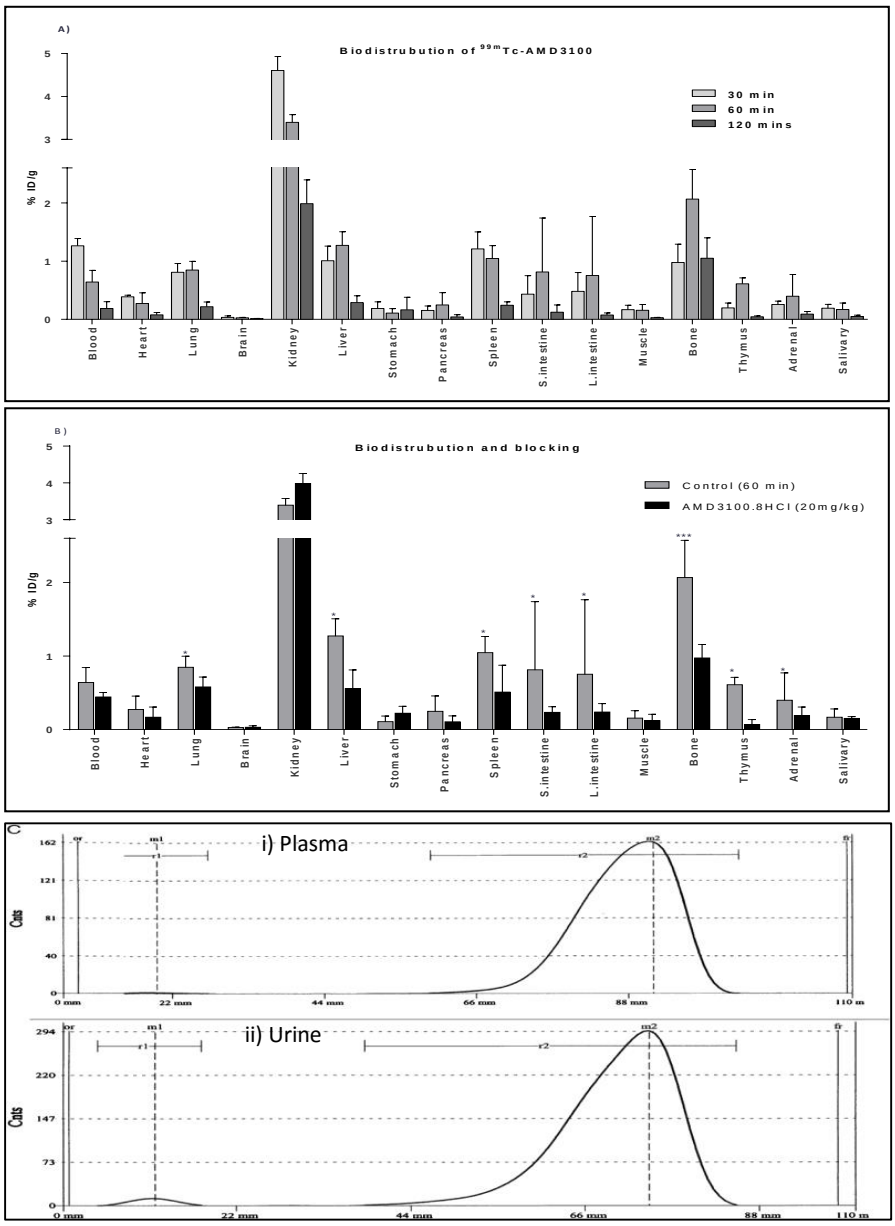

Figure- 5: A) Biodistribution data of selected organs from the normal Balb/*c* mice injected with 5 MBq [^{99m}Tc]O_2-AMD3100 and terminated at different time points. Biodistribution data are represented as mean ± SD of 4 animals. B) *Ex vivo* biodistribution and blocking studies of [^{99m}Tc]O_2-AMD3100 in normal Balb/*c* mice at 1 h after tracer injection with or without blocking dose of AMD3100.8HCl (20 mg/kg). Data are represented as mean ± SD, *($p < 0.05$), ***($p < 0.001$) statistical analysis was performed by unpaired by two-tailed students t-test. C) Typical radio-TLC analysis of [^{99m}Tc]O_2-AMD3100 using Whatman No. 3 paper and saline as the eluent. Two hours post injection the tracer was found to be stable in i) plasma (98% intact) and ii) urine (97% intact).

When an excess of unlabelled AMD3100 was injected prior to [^{99m}Tc]O_2-AMD3100 injection, nonspecific uptake in the kidneys was increased further, indicating that after blocking of the receptor, a greater fraction of the injected dose is cleared via the kidneys. The tracer was stable *in vivo*, as plasma and urine analysis by TLC showed that the tracer remained intact in plasma (> 98%) for 2 h and was eliminated as intact tracer (> 97%) into the urine (Fig-5C).

Immunohistochemistry

The morphological analysis of the xenografts revealed viable tumor tissue, with a few cells undergoing mitosis. In order to verify the presence of CXCR4 in PC-3 tumor xenografts, we performed immunostaining of the resected tumors. The moderate cytoplasmic expression of CXCR4 protein was found to be homogeneously distributed throughout the tumor. For comparison, immunohistochemistry was also performed on liver, lungs, spleen, intestine and pancreas. Staining reveled a strong to moderate homogenous expression of CXCR4 in liver, lung, intestine and spleen, but not in the pancreas. The tissues that expressed CXCR4, as determined by immunohistochemistry also showed specific tracer uptake in the *ex-vivo* biodistribution study (Fig- 6).

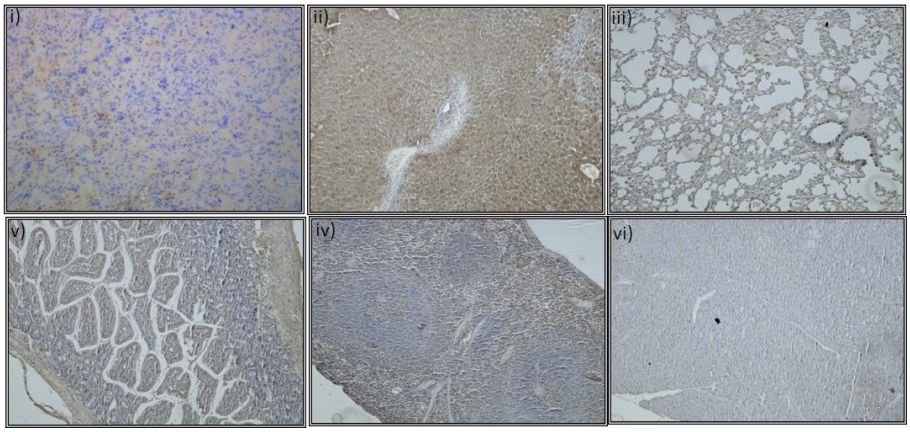

Figure- 6: Immunohistochemistry demonstrating the expression of CXCR4 protein in various organs: i) PC-3 tumor, ii) liver, iii) lung iv) spleen v) small intestine and vi) pancreas. All the tissues were found to be positive whereas pancreas showed negative.

SPECT Imaging

Typical [^{99m}Tc]O_2-AMD3100 small animal SPECT images of mice bearing PC-3 tumors are presented in Fig-7. Based on the biodistribution studies, a dynamic scan of 60 min of the tumor region was acquired, followed by a 10 min whole body scan. Scans were acquired with and without prior administration of an excess of unlabelled AMD3100. Prominent accumulation of tracer was seen in the tumor in all the frames of the dynamic SPECT scan in the absence of a blocking agent. In addition, high uptake was also seen in liver, spleen, and lungs. Injection of an excess of the blocking agent prior to tracer injection reduced the uptake in tumor and other CXCR4 positive organs, while kidneys remained visible.

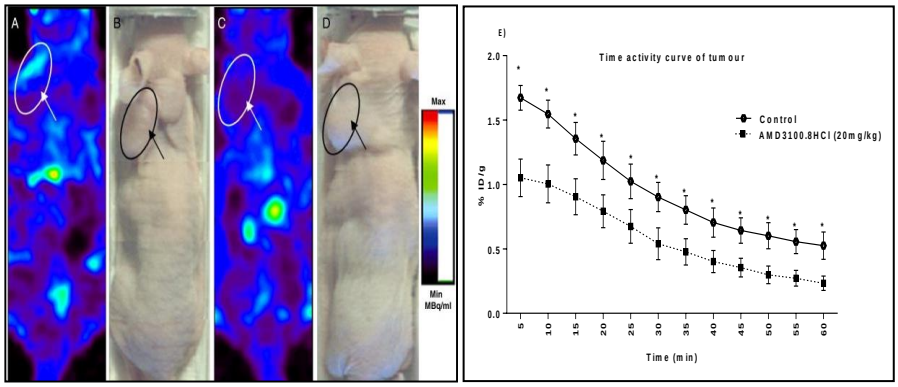

Figure-7: CXCR4 imaging in PC-3 tumor xenografts bearing mice with [^{99m}Tc]O_2-AMD3100. Tracer was injected through penile vein, and whole body images were acquired at 70 min post injection. Coronal view of an *athymic* nude mice bearing a tumor, A) control SPECT of a control animal B) digital image of control animal. C) SPECT image after administration of a blocking dose of AMD3100.8HCl (20 mg/kg). D) Digital image of the blocked mice. Arrow indicates the tumor. E) Time-activity curves of PC-3 tumors in tumor-bearing mice, acquired by SPECT between 5 and 60 min post injection of [^{99m}Tc]O_2-AMD3100. The ROI values were corrected for the injected dose and converted to % ID/g and expressed as mean ± SEM of 5 animals, * (p< 0.05).

Time activity curves were generated from the SPECT images, regions of interest (ROIs) were drawn around the tumors and the amount of radioactivity in the ROIs was quantified and converted to % ID/g. The data showed a different kinetic behaviour of the tracer in tumor between control and AMD3100-treated mice (Fig-7E). In the tumor of control mice, the highest accumulation of the tracer was reached within 5 min post injection, subsequently activity decreased exponentially.

In case of AMD3100-treated animals, the initial tracer uptake was lower than in controls, but the tracer showed similar washout. The difference in tracer uptake between both groups of animals was statistically significant at all the time points ($p < 0.05$). Furthermore, the area under the curve (AUC) of the control tumor (5–60 min) was 11.1 ± 2.4 min, which is significantly higher than the AUC of the AMD3100-treated tumor 6.6 ± 1.6 min ($p < 0.05$).

DISCUSSION

Because of its availability from generator systems and the relative easy of radiometallation chemistry, the SPECT agent ^{99m}Tc has gained wide interest in the field of radiopharmaceutical chemistry. In this study, we aimed to radiolabel the drug AMD3100 with ^{99m}Tc and evaluate it as a potential tracer for SPECT imaging. After optimization of the procedure, AMD3100 was readily labelled, giving [^{99m}Tc]O_2-AMD3100 in high yield. The AMD3100 has cyclam ring which is similar to the DOTA or NOTA ring structure and suitable for the radiometal chemistry. Recently, a copper [^{64}Cu] labelled AMD3100 has been evaluated as a PET tracer [35,37]. However, the radiosynthesis was relatively time-consuming and *in-vitro* binding assay in Jurkat cells resulted in IC_{50} value in micromolar range. Generally, the copper complexes are thermodynamically unstable and are more prone to release the metal ion *in vivo*; as a result most of copper binds to plasma protein and give high background.

We anticipated that the incorporation of the ^{99m}Tc metal ions into the cyclam ring would increase the binding affinity of the AMD3100 towards CXCR4. However, the *in vitro* binding study showed nearly a 3 fold higher IC_{50} value in the homologous binding assay with [^{99m}Tc]O_2-AMD3100, in comparison to the reported values for [^{64}Cu]$^{2+}$-AMD3100 [35]. In line with this it was demonstrated that the incorporation of a transition metal ions, such as Ni^{2+}, Zn^{2+} and Cu^{2+}, into the macrocyclic rings of cyclams and bicyclams enhances the binding affinity for the CXCR4 receptors by 50, 36 and 7 fold respectively, whereas incorporation of bigger metal ions, such as Pd^{2+}, decreases the binding affinity of AMD3100 [43]. This may be the reason for the reduced IC_{50} values in the homologous binding assay, as compared to the Cu^{2+} complex. Since Cu^{2+}increases the binding affinity of AMD3100 to CXCR4 by 7

fold, the 3 fold decrease in IC_{50} of $[^{99m}Tc]O_2$-AMD3100 compared to the Cu^{2+} complex indicates that incorporation of TcO^{+}_{2} still increases the binding affinity of labelled AMD3100 compared to free AMD3100. Thus, we anticipated that the binding affinity of $[^{99m}Tc]O_2$-AMD3100 is sufficient to warrant further evaluation *in vivo*.

Our tracer was found to be stable both *in vitro* and *in vivo*. The transchelation to cysteine is a principle main reason for *in vivo* instability of most of ^{99m}Tc-labelled tracers. In our case, the $[^{99m}Tc]O_2$-AMD3100 was stable even at higher molar ratio of cysteine and displayed thermodynamical stability. The uptake of tracer was observed in liver, bone marrow, lymph nodes, spleen, intestine and thymus. It has been reported that these organs express relatively high levels of the CXCL12 ligand, and consequently accumulate high number of CXCR4-positive cells, such as hematopoietic stem/progenitor or immune cells. CXCR4 expression in these organs was confirmed by immunostaining [25,50-55]. The blocking experiment shows that accumulation in these tissues was specific. Moreover, we observed negligible tracer uptake in the brain, even though brain has relatively high expression of CXCR4 receptors, which is due to the polar nature of the tracer [9]. The tracer uptake in most CXCR4 poor organs decreased with time, with the exception of kidney and bladder. This indicates that the tracer was mainly excreted via the renal pathway, as could be expected based on its high hydrophilicity. After 2 h, most radioactivity was cleared from the body as intact tracer, as no radioactive metabolites were found in urine. Previous preclinical studies have also shown that, the native AMD3100 has fast pharmacokinetics and is eliminated unchanged through the renal route [40, 56].

Based on the biodistribution data, an imaging study was performed in prostate tumor xenografted mice. We selected the PC-3 prostate cancer model, because this tumor cell line has constitutive expression of CXCR4 receptors [57]. The moderate basal expression of CXCR4 in these cells better reflects the normal physiology in a clinical situation than the genetically engineered tumors with high overexpression of CXCR4 that are frequently used in this field of research. SPECT imaging could clearly visualize the accumulation of the tracer in the tumor. The imaging study also

demonstrated the [^{99m}Tc]O_2-AMD3100 uptake was specifically receptor mediated, as the accumulation was blocked by an excess of cold AMD3100. The specific accumulation of the tracer in tumor tissue was supported by immunostaining of tumor sections, showing homogenous CXCR4 expression in the tumor. Tumor time–activity curves of the control and AMD3100-treated animals also confirmed specific binding of [^{99m}Tc]O_2-AMD3100, as the AUC of the control tumors is 1.7 times higher when compared to the AUC of AMD3100 saturated tumors (p <0.05). Apart from the tumor, a high uptake of the tracer was also observed in liver and lungs, due to the relatively high basal expression of CXCR4 in these organs, indicating that [^{99m}Tc]O_2-AMD3100 may not be suitable for diagnosis of lung and liver metastasis. *Ex vivo* biodistribution data of the previously published [^{64}Cu]$^{2+}$-AMD3100 were slightly different from the data for [^{99m}Tc]O_2-AMD3100 obtained in our study, indicating that the radio-isotope does affect the *in vivo* properties of the tracer. For [^{64}Cu]$^{2+}$-AMD3100, accumulation of tracer increased over a longer period of time in all tissues especially in the liver and lymph nodes (up to 6 h), whereas accumulation of [^{99m}Tc]O_2-AMD3100 reaches a maximum at 1 h. This might be explained by the lower binding affinity of the technetium complex and a faster clearance rate [35].

CONCLUSION

The *ex-vivo* biodistribution and SPECT studies have revealed that [^{99m}Tc]O_2-AMD3100 primarily accumulates in organs with high expression of CXCR4 and that *in vivo* tracer accumulation in these organs is specific. In addition, the tracer is easy to prepare and technetium-99m is widely available and inexpensive. These aspects justify further evaluation of this radiopharmaceutical as a potential marker for the non-invasive imaging of CXCR4 receptors.

REFERENCES

1. Bleul C, Schultze JL, Springer TA. **B lymphocyte chemotaxis regulated in association with microanatomic localization, differentiation state and B cell receptor engagement**. *Journal of Experimental Medicine*. 1998; 187:753-62.
2. Nagasawa T**. Defects of B-cell lymphopoiesis and bone marrow myelopoiesis in mice lacking the CXC chemokine PBSF/SDF-1**. *Nature.* 1996; 382:635-48.
3. Ma Q, Jones D, Borghesani PR, Segal RA, Nagasawa T, Kishimoto T, Bronson RT, Springer TA. **Impaired B lymphopoiesis, myelopoiesis and derailed cerebellar neuronal migration in CXCR4 and SDF-1 deficient mice**. *Proc. Natl. Acad. Sci.* 1998;95:9448-53.
4. Unutmaz D, Littman DR. **Expression pattern of HIV-1 coreceptors on T cells: Implications for viral transmission and lymphocyte homing**. *Proc.Natl.Acad.Sci*. 1997; 94:1615-28.
5. Nagasawa T, Tachibana K, Kishimoto T. **A novel CXC chemokine PBSF/SDF-1 and its receptor CXCR4: their functions in development, hematopoiesis and HIV infection**. *Seminars in Immunology*. 1998; 10:179-85.
6. Fran B. **The significance of cancer cell expression of the chemokine receptor CXCR4.** *Seminars in Cancer Biology*. 2004;14:171-79.
7. Liang Z, Brooks J, Willard M, Liang K, Yoon Y, Kang S, Shim H. **CXCR4/CXCL12 axis promotes VEGF-mediated tumor angiogenesis through Akt signaling pathway.** *Biochemistry & Biophysics Research Communication.* 2007; 359:716-22.
8. Mélik-Parsadaniantz S, Rostène W. **Chemokines and neuromodulation.** *Journal of Neuroimmunology*. 2008;198:62-48.
9. Banisadr G, Fontanges P, Haour F, Kitabgi P, Rostène W, Mélik Parsadaniantz S. **Neuroanatomical distribution of CXCR4 in adult rat brain and its localization in cholinergic and dopaminergic neurons.** *European Journal of Neuroscience*. 2002; 16:1661-71.
10. Rostene W, Kitabgi P, Parsadaniantz SM. **Chemokines: a new class of neuromodulator?** *Nature Reviews Neurosciences.* 2007; 8: 895-03.
11. Zou YR, Kottmann AH, Kuroda M, Taniuchi I, Littman DR. **Function of chemokine receptor CXCR4 in haematopoiesis and in cerebellar development.** *Nature.* 1998; 393:595-9.
12. Lu M, Grove EA, Miller RJ. **Abnormal development of the hippocampal dentate gyrus in mice lacking the CXCR4 chemokine receptor.** *Proc. Natl Acad. Sci.* 2002; 99:7090-5.
13. Gerard C, Rollins BJ. **Chemokines and disease**. *Nature Immunology*. 2001;2:108-15.
14. Premack BA, Schall TJ. **Chemokine receptors: Gateways to inflammation and infection.** *Nature Medicine.* 1996; 2:1174-78.
15. Murdoch C, Finn A. **Chemokine receptors and their role in inflammation and infectious diseases.** *Blood*. 2000; 95:3032-43.
16. Berger EA, Murphy PM, Farber JM. **Chemokine receptors as HIV-1 coreceptors: Roles in Viral Entry, Tropism, and Disease.** *Annual Review of Immunology.* 1999; 17:657-700.
17. Kaul M, Garden GA, Lipton SA. **Pathways to neuronal injury and apoptosis in HIV associated dementia.** *Nature*. 2001; 410:988-94.
18. Power C, Johnson RT. **Neuroimmune and neurovirological aspects of human immunodeficiency virus infection Advances in Virus Research**. *Academic Press*. pp. 389-33.
19. McArthur JC, Haughey N, Gartner S, Conant K, Pardo C, Nath A, Sacktor N. **Human Immunodeficiency Virus-Associated Dementia: An Evolving Disease.** *Journal of Neurovirology.* 2003; 9:205-21.
20. Burger JA, Kipps TJ. **CXCR4: A key receptor in the cross talk between tumor cells and their microenvironment.** *Blood.* 2005; 107(5):1761-67.
21. Tanaka T, Bai Z, Srinoulprasert Y, Yang B, Hayasaka H, Miyasaka M. **Chemokines in tumor progression and metastasis.** *Cancer Science.* 2005; 96:317-22.

22. Muller A, et al. **Involvement of chemokine receptors in breast cancer metastasis.** *Nature.* 2001; 410:50-56.
23. Xiang Z, Zeng Z, Tang Z, Fan J, Zhuang P, Liang Y, Tan Y, He J. **Chemokine receptor CXCR4 expression in hepatocellular carcinoma patients increases the risk of bone metastases and poor survival.** *BMC Cancer.* 2009;9:176
24. Zeelenberg IS, Ruuls-Van Stalle L, Roos E. **The Chemokine Receptor CXCR4 Is Required for Outgrowth of Colon Carcinoma Micrometastases.** *Cancer Research.* 2003; 63:3833-39.
25. Kato M, Kitayama J, Kazama S, Nagawa H. **Expression pattern of CXC chemokine receptor-4 is correlated with lymph node metastasis in human invasive ductal carcinoma**. *Breast Cancer Research.* 2003; 5:R144-50.
26. Cabioglu N, et al. **Chemokine receptor CXCR4 expression in breast cancer as a potential predictive marker of isolated tumor cells in bone marrow.** *Clinical and Experimental Metastasis.* 2005; 22:39-46.
27. Cabioglu N, Yazici MS, Arun B, Broglio KR, Hortobagyi GN, Price JE, Sahin A. **CCR7 and CXCR4 as Novel Biomarkers Predicting Axillary Lymph Node Metastasis in T1 Breast Cancer.** *Clinical Cancer Research.* 2005; 11:5686-93.
28. Zlotnik A, Burkhardt AM, Homey B. **Homeostatic chemokine receptors and organ-specific metastasis.** *Nature Reviews of Immunology.* 2011; 11:597-06.
29. Murakami T, Maki W, Cardones AR, Fang H, Tun Kyi A, Nestle FO, Hwang ST. **Expression of CXC Chemokine Receptor-4 Enhances the Pulmonary Metastatic Potential of Murine B16 Melanoma Cells.** *Cancer Research.* 2002; 62:7328-34.
30. Tamamura H, et al. **T140 analogs as CXCR4 antagonists identified as anti-metastatic agents in the treatment of breast cancer.** *FEBS Letters.* 2003; 550:79-83.
31. Liang Z, Wu T, Lou H, Yu X, Taichman RS, Lau SK, Nie S, Umbreit J, Shim H. **Inhibition of Breast Cancer Metastasis by Selective Synthetic Polypeptide against CXCR4**. *Cancer Research.* 2004; 64:4302-08.
32. Amine A, et al. **Novel Anti-Metastatic Action of Cidofovir Mediated by Inhibition of E6/E7, CXCR4 and Rho/ROCK Signaling in HPV+ Tumor Cells.** *PLoS ONE:* e5018.
33. Nimmagadda S, Pullambhatla M, Pomper MG**. Immunoimaging of CXCR4 Expression in Brain Tumor Xenografts Using SPECT/CT.** *Journal of Nuclear Medicine.* 2009;50:1124-30.
34. Hanaoka H, et al. **Development of a 111In-labeled peptide derivative targeting a chemokine receptor, CXCR4, for imaging tumors.** *Nuclear Medicine and Biology.* 2006; 33:489-94.
35. Jacobson O, Weiss ID, Szajek L, Farber JM, Kiesewetter DO. **[64Cu]-AMD3100—A novel imaging agent for targeting chemokine receptor CXCR4.** *Bioorganic & Medicinal Chemistry.* 2009; 17:1486-93.
36. Jacobson O, Weiss ID, Kiesewetter DO, Farber JM, Chen X. **PET of Tumor CXCR4 Expression with 4-18F-T140.** *Journal of Nuclear Medicine.* 2010; 51:1796-04.
37. Nimmagadda S, Pullambhatla M, Stone K, Green G, Bhujwalla ZM, Pomper MG. **Molecular imaging of CXCR4 receptor expression in human cancer xenografts with [64Cu]AMD3100 positron emission tomography.** *Cancer Research.* 2010; 70:3935–44.
38. Bridger GJ, et al. **Synthesis and Structure–Activity Relationships of Phenylenebis(methylene)-Linked Bis-tetraazamacrocycles That Inhibit Human Immunodeficiency Virus Replication. 2. Effect of Heteroaromatic Linkers on the Activity of Bicyclams.** *Journal of Medicinal Chemistry.* 1996;39:109-19.
39. Hendrix CW, et al. **Safety, Pharmacokinetics, and Antiviral Activity of AMD3100, a Selective CXCR4 Receptor Inhibitor, in HIV-1 Infection**. *Journal of Acquired Immune Deficiency Syndromes.* 2004; 37:1253-62.
40. Liles WC, et al. **Mobilization of hematopoietic progenitor cells in healthy volunteers by AMD3100, a CXCR4 antagonist.** *Blood.* 2003; 102:2728-30.

41. Hübel K, et al. **Leukocytosis and Mobilization of CD34+ Hematopoietic Progenitor Cells by AMD3100, a CXCR4 Antagonist.** *Supportive Cancer Therapy.* 2004; 1:165-72.
42. Lukacs NW, Berlin A, Schols D, Skerlj RT, Bridger GJ. **AMD3100, a CXCR4 antagonist, attenuates allergic lung inflammation and airway hyperreactivity.** *American Journal of Pathology*. 2002; 160:1353-60.
43. Gerlach LO, Jakobsen JS, Jensen KP, Rosenkilde MR, Skerlj RT, Ryde U, Bridger GJ, Schwartz TW. **Metal Ion Enhanced Binding of AMD3100 to Asp262 in the CXCR4 Receptor†.** *Biochemistry*. 2002; 42:710-17.
44. Zhang JM, Tian JH, Li TR, Guo HY, Shen L. **99mTc–AMD3100: A novel potential receptor-targeting radiopharmaceutical for tumor imaging.** *Chinese Chemical Letters*. 2010;21:461-63.
45. Bridger GJ, et al. **Synthesis and Structure-Activity Relationships of Phenylenebis (methylene)-Linked Bis-Tetraazamacrocycles That Inhibit HIV Replication. Effects of Macrocyclic Ring Size and Substituents on the Aromatic Linker.** *Journal of Medicinal Chemistry*. 1995; 38:366-78.
46. CM Giandomencio WY. **Process for preparation of N-1 protected N ring nitrogen containing cyclic polyamines and products thereof**. *WO 2002026721 A1*. 2002; 09/970,288:294859
47. Sinn HJ, Schrenk HH, Friedrich EA, Via DP, Dresel HA. **Radioiodination of proteins and lipoproteins using N-bromosuccinimide as oxidizing agent.** *Analytical Biochemistry*. 1988;170:186-92.
48. Jacobson O, Weiss ID, Szajek LP, Niu G, Ma Y, Kiesewetter DO, Farber JM, Chen X. **PET imaging of CXCR4 using copper-64 labeled peptide antagonist.** *Theranostics*. 2011; 1:251-62.
49. Troutner DE, Simon J, Ketring AR, Volkert W, Holmes RA. **Complexing of Tc-99m with Cyclam: Concise Communication.** *Journal of Nuclear Medicine.* 1980; 21:443-48.
50. Volkert.richard A Holmes. **Biodistribution of Liphophilic 99mTc comples of cyclam Derivatives.** *International Journal of Nuclear Medicine and Biology*.1984; 11(2):113-19.
51. Wald O, et al. **Involvement of the CXCL12/CXCR4 pathway in the advanced liver disease that is associated with hepatitis C virus or hepatitis B virus.** *European Journal of Immunology*. 2004; 34:1164-74.
52. Shibuta K, Mori M, Shimoda K, Inoue H, Mitra P, Barnard GF. **Regional Expression of CXCL12/CXCR4 in Liver and Hepatocellular Carcinoma and Cell-cycle Variation during in vitro Differentiation.** *Cancer Science.* 2002; 93:789-97.
53. Zhao X, Qian D, Wu N, Yin Y, Chen J, Cui B, Huang L. **The spleen recruits endothelial progenitor cell via SDF-1/CXCR4 axis in mice.** *Journal of Receptors and Signal Transduction.* 2010; 30:246-54.
54. Moll NM, Ransohoff RM. **CXCL12 and CXCR4 in bone marrow physiology**. *Expert Reviews of Hematology.* 2010; 3:315-22.
55. Tachibana K. **The chemokine receptor CXCR4 is essential for vascularization of the gastrointestinal tract**. *Nature.* 1998; 393:591-94.
56. Hendrix CW, et al. **Pharmacokinetics and Safety of AMD-3100, a Novel Antagonist of the CXCR-4 Chemokine Receptor, in Human Volunteers.** *Antimicrobial Agents and Chemotherapy.* 2000; 44:1667-73.
57. Singh S, Singh UP, Grizzle WE, Lillard JW. **CXCL12-CXCR4 interactions modulate prostate cancer cell migration, metalloproteinase expression and invasion.** *Laboratory Investigation.*2004; 84:1666-76.